JOURNAL OF MATERIALS SCIENCE 39 (2004) 895–901

A study on the growth of TiO_2 nanorods using sol electrophoresis

S. J. LIMMER, T. P. CHOU, G. Z. CAO
University of Washington, Department of Materials Science and Engineering & Center for Nanotechnology, 302 Roberts Hall, Box 352120, Seattle, WA 98195, USA
E-mail: sjlimmer@u.washington.edu

This article presents a study on the growth process for the template-based growth of TiO_2 nanorods by sol electrophoretic deposition, through both experiment and simulation. Uniformly sized nanorods of approximately 45–200 nm in diameter and 10–60 μm in length can be grown over large areas with near unidirectional alignment. The nanorods have the desired stoichiometric chemical composition and anatase crystal structure, after firing to 500°C for 1 h. These nanorods have also been formed into parallel arrays on a substrate, such as indium-tin oxide (ITO) glass. The current flowing though the deposition cell has been measured, to gain insights into the growth process. Additionally, a model has been used to calculate the currents, to compare the expected growth behavior with the experimental results. Relations between processing conditions, growth parameters and the morphologies of nanorods are discussed.

1. Introduction

Metal oxides, particularly complex metal oxides, are important materials for various applications. Examples include transparent conducting oxides for light-emitting devices [1], complex oxide sensors and catalysts [2] and TiO_2 solar cells [3]. For many applications of metal oxides, the sensitivity or efficiency obtained is directly proportional to the surface area of the material. Nanorods or nanowires offer a significantly larger surface area compared to that of films or the bulk material. Nanorods or nanowires also offer the opportunity to study the physical properties of one-dimensional structures. Many researchers study oxide nanorod synthesis, and a number of different synthesis techniques have been developed. Examples include oxidation of metallic nanorods [4], vapor-liquid-solid (VLS) growth [5], and the filling of templates with colloidal oxide particles [6]. There are some limitations and difficulties with these techniques, however. Direct oxidation is generally limited to formation of simple metal oxide nanorods. VLS growth of oxide nanorods and nanowires is restricted to systems that can form a eutectic liquid with the catalyst at the (often very high) growth temperature. Colloidal dispersion filling of templates offers simple fabrication of nanorods, and the possibility of fabrication of complex oxide nanorods with precise control of stoichiometric composition. However, complete filling of solids inside holes could be challenging, considering the fact that typical sols or colloidal dispersions consist of 90 percent or more solvent. In fact, the structures synthesized by this technique are often hollow tubes rather than solid rods [6, 7]. Our research focuses on a novel approach for synthesis and fabrication of nanorods of complex oxides. This approach combines sol-gel processing, electrophoretic deposition and template-based growth. This method offers the possibility of making nanorods of any complex oxides, organic-inorganic hybrids and bio-inorganic hybrids. In addition, this technique would allow the fabrication of unidirectionally aligned and uniformly sized nanorods with desired patterns for device fabrication, physical property measurements and characterization.

Sol-gel processing is a wet chemical route for the synthesis and processing of inorganic and organic-inorganic hybrid materials. Sol-gel processing offers many advantages, including low processing temperatures (typically <100°C) and molecular level homogeneity, and it is particularly useful in making complex metal oxides. Typical sol-gel processing consists of hydrolysis and condensation of precursors. Precursors can be either organic, such as metal alkoxides, or inorganic salts. Organic or aqueous solvents may be used to dissolve precursors, and catalysts are often added to promote and/or control both hydrolysis and condensation reactions. Hydrolysis and condensation reactions are both multiple-step processes, occurring sequentially and in parallel. Condensation results in the formation of nanoscale clusters of metal oxides and hydroxides, often with organic groups attached to them. These organic groups may be due to incomplete hydrolysis, or introduced as non-hydrolyzable organic ligands. Sol-gel processing results in the formation of nanoscale clusters of metal oxides and hydroxides, whose size can be tailored by controlling the hydrolysis and condensation reactions. By careful control of sol preparation and processing, monodispersed nanoscale particles can be synthesized. The particle size can be varied by changing the concentration and aging time [8]. In a typical sol, nanoclusters formed by hydrolysis and condensation reactions commonly have a size ranging from 1

to 100 nm. These clusters are often electrostatically stabilized.

Upon application of an external electric field to a sol, the constituent charged particles undergo electrophoresis. The mobility of a nanoparticle in a sol is dependent on the dielectric constant of the liquid medium, the zeta potential of the nanoparticle, and the viscosity of the fluid. Sol electrophoretic deposition simply uses this motion of charged sol particles to grow films or monoliths. At the electrodes, surface electrochemical reactions proceed to generate or receive electrons. The electrostatic double layers collapse upon deposition on the growth surface, and the particles coagulate. The films or monoliths grown by sol electrophoretic deposition are essentially a compaction of nanosized particles. Such films or monoliths are porous, i.e., there are voids inside. Typical packing densities, defined as the fraction of solid (also called green density) are less than 74%, which is the highest packing density for uniformly sized spherical particles [9]. The green density of films or monoliths by sol electrophoretic deposition is strongly dependent on the concentration of particles in the sol, zeta-potential, externally applied electric field and reaction kinetics between particle surfaces. Slow reaction and slow arrival of nanoparticles on the surface would allow sufficient particle relaxation on the deposition surface, so that a high packing density is expected.

We have previously reported that $BaTiO_3$, SiO_2, $Sr_2Nb_2O_7$ and PZT nanorods can be grown by sol-gel electrophoresis [10, 11]. The length of all theserods is about 10 μm, similar to the thickness of the template membrane. For samples grown in 200 nm templates, the final diameters were about 150 nm for $BaTiO_3$, $\sim$200 nm for SiO_2, $\sim$125 nm for $Sr_2Nb_2O_7$ and $\sim$150 nm for PZT. The corresponding shrinkages are approximately 25, 0, 37 and 25%. The composition of a material formed by this technique will consist of the desired crystalline phase with the desired stoichiometry, as we have recently demonstrated, for example, in nanorods of the complex oxide $Pb(Zr,Ti)O_3$ (PZT) [10]. XRD spectra of the PZT nanorods show only the desired phase, with no shifts in peak positions or intensity ratios with respect to bulk PZT [10]. This gives an idea of the possibilities inherent to sol electrophoretic growth of nanorods.

In this paper, we present a study on the growth of TiO_2 nanorods using the sol electrophoretic technique. Nanorods of various sizes are demonstrated, along with arrays of nanorods aligned on a surface. In addition, the growth process is examined through both experiment and simulation. Current evolution recorded during nanorod growth is compared with calculated values from a model for the electrophoretic deposition.

2. Experimental

A combination of sol-gel processing and electrophoretic deposition has been used to synthesize a variety of oxide nanorods, similar to the process reported previously [10, 11]. Briefly, the sols were prepared as follows. TiO_2 sol was formed by dissolving titanium (IV) isopropoxide in glacial acetic acid, followed by the addition of deionized (DI) water. Upon addition of water, a white precipitate instantaneously formed. However, the sol became a clear liquid after $\sim$5 min of stirring.

Nanorod growth occurred on a working electrode of aluminum, with a Pt mesh counter electrode. The template membranes used for growth of the nanorods were track-etched hydrophilic polycarbonate (Millipore Isopore), with pore diameters of 50–200 nm, and a thickness of 10 μm, or 60 μm thick anodic alumina (Whatman Anodisc), with 200 nm pores. The polycarbonate (PC) membrane and the working electrode are placed in a polypropylene filter holder, and held in place with a silicone gasket. This assembly is placed in contact with the sol. A Pt counter electrode is also placed in the sol, parallel to the working electrode. A slightly different arrangement was used with anodic alumina templates. Indium-tin-oxide (ITO) glass was used as the working electrode and Pt mesh was used as the counter electrode. The alumina membrane contacting the conducting substrate is immersed in the sol parallel to the Pt counter electrode approximately 2.5 cm apart. The sol is initially drawn into the membrane pores by capillary action after membrane immersion into the sol. For electrophoretic growth, a potential of 5 V is applied between the electrodes, and held for up to 60 min for the polycarbonate membrane or up to 3 h for the alumina membrane. At the end of electrophoretic deposition, excess sol is blotted off the membrane. Samples prepared in this manner are dried at $\sim$100°C for several hours, then placed in an oven and fired for 60 min at 500°C. This is to burn off the polycarbonate membranes, to make the nanorods dense, and to crystallize the sol in the desired (anatase) phase. Additional wet chemical etching with 6 M NaOH is required to remove the alumina membrane since alumina withstands high temperatures, and epoxy adhesive is used to aid in the attachment of nanorods on ITO conducting substrates.

The current flowing through the deposition cell was recorded with a data acquisition board (National Instruments PCI-6024E) connected to a computer running LabVIEW software (National Instruments). Scanning electron microscopy (SEM, JEOL 840A) and transmission electron microscopy (TEM, JEOL 2010) were used to study the morphology and crystallinity of the nanorods. Samples were sputter-coated with a thin Au/Pd layer prior to observation in the SEM. X-ray diffraction (XRD, Phillips PW1830) was used to determine the phases and crystal structures present, and to check for the presence of texture and degree of crystallinity.

3. Results and discussion

Figs 1–3 shows sample results obtained for TiO_2 nanorods. SEM micrographs of two different sizes of TiO_2 nanorods grown in a polycarbonate membrane by sol-gel electrophoresis are shown in Fig. 1. These nanorods have a uniform diameter and smooth surface throughout their entire length. Comparing the various rods in each image, one can see that they all have roughly the same length and diameter. These images show that the rods are roughly parallel to one another over a large area. The diameters of the TiO_2 nanorods

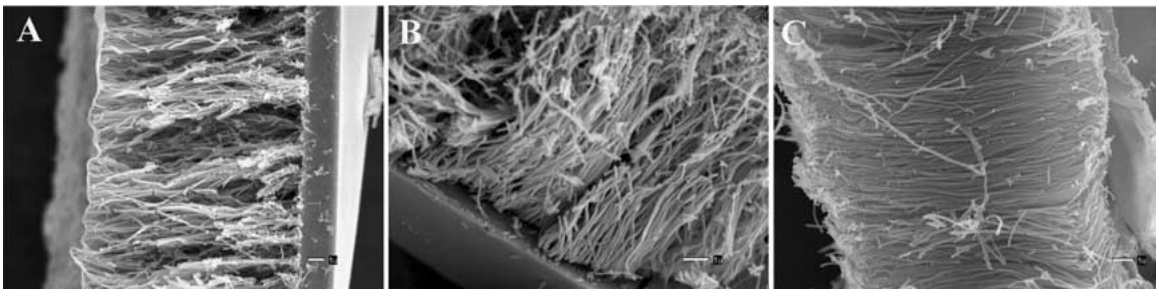

Figure 1 SEM micrographs of different sizes of TiO_2 nanorods grown in a polycarbonate membrane by sol electrophoretic deposition. The diameters of the nanorods are approximately: (A) 180 nm (for the 200 nm template), (B) 90 nm (for the 100 nm template), and (C) 45 nm (for the 50 nm template).

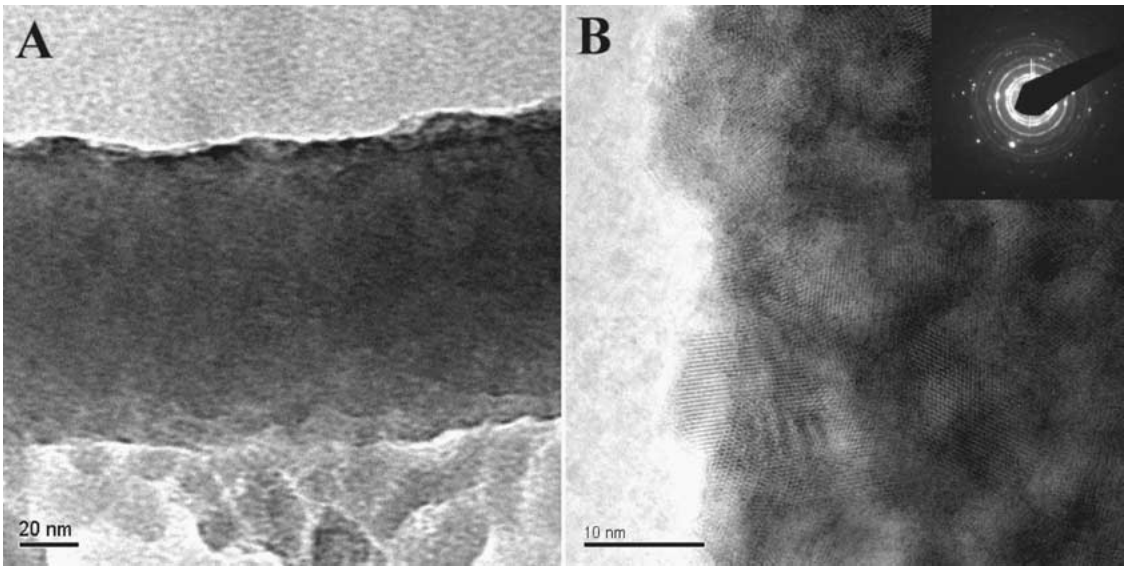

Figure 2 Part A shows a TEM micrograph of a TiO_2 nanorod, demonstrating that the nanorods are quite smooth and dense. Part B shows a high-resolution TEM image and electron diffraction pattern, demonstrating that the nanorods are polycrystalline, with grains ~5 nm in size.

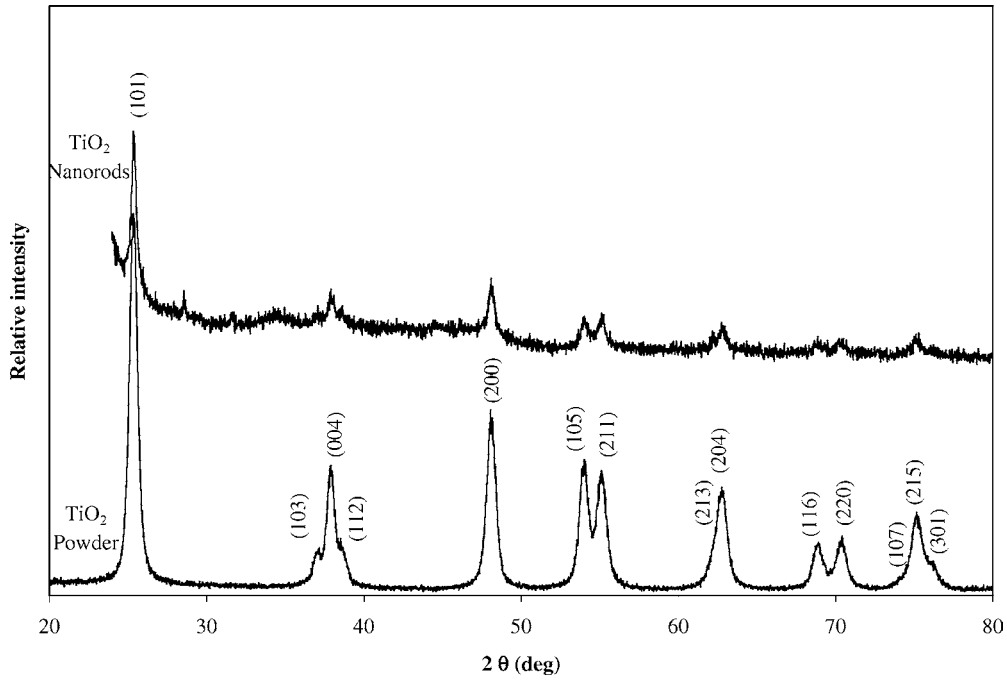

Figure 3 Part F shows XRD spectra of both the grown TiO_2 nanorods and a powder derived from the same sol. Both samples consist of the anatase phase, and there is no observed shift in the peak positions for the nanorod sample. In addition, the relative intensities of the peaks are the same for the nanorod sample, showing that there is no preferred orientation in the nanorods.

are estimated to be ∼180 nm (for the 200 nm template), ∼90 nm (for the 100 nm template), and ∼45 nm (for the 50 nm template). This corresponds to approximately 10 percent lateral shrinkage with respect to the membrane pore diameter. This size difference is most likely due to the volume shrinkage caused by densification during the heat treatment. Fig. 2A shows a TEM micrograph of a TiO_2 nanorod, demonstrating that the nanorods are quite smooth and dense. Fig. 2B shows a high-resolution TEM image and electron diffraction pattern, demonstrating that the nanorods are polycrystalline, with grains that are ∼5 nm in size. XRD spectra of the TiO_2 rods are shown in Fig. 3, along with the spectra for a powder formed from the same sol and fired at 500°C for 60 min. From the powder XRD spectrum, it can be seen that the sample consists entirely of the anatase phase. Comparison of the two spectra shows that there are identical peaks in both samples. Further, the peak positions are the same and the intensity ratios among various peaks are similar. Note that there is a large amorphous background associated with the TiO_2 nanorods. This is due to the small volume of rods available for analysis, meaning that much of the X-ray beam was hitting the (amorphous) sample holder. For the TiO_2 rods grown in 50 nm templates, it was found that the drying time used has a strong influence on the fidelity of the nanorods. When the samples were dried at 100°C for times up to 24 h, no nanorods were observed after firing at 500°C. However, if the samples were dried for ∼48 h prior to firing, nanorods were observed. It is likely that this result is due to the increased degree of condensation that occurred in the sample dried for a longer time. By allowing the samples to undergo further condensation reactions, the rods formed were likely stronger, and thus better able to resist breakage upon firing.

TiO_2 nanorods grown and attached on conducting substrates, specifically on ITO glass, have also been investigated. These initial results show favorable potential for possible use in a wide spectrum of applications such as chemical and biological sensors [12] and two-dimensional photonic bandgap crystals [13], allowing for most conventional methods to be used for determining the physical properties of these nanoscale materials. Fig. 4A shows arrays of TiO_2 nanorods attached to ITO glass using alumina membranes, indicating extensive surface coverage of these nanorods on the substrate. The arrays of TiO_2 nanorods are shown from the top view, indicating that the nanorods are fairly free-standing on the substrate and aligned unidirectionally. Fig. 4B shows a closer view of individual nanorods grown by sol electrophoresis in an alumina membrane after partial membrane removal by wet chemical etching. The nanorods grown are approximately 200 nanometers in diameter and 30 to 40 microns in length, running perpendicular to the substrate. These alumina membranes allow for 500°C sintering, densifying the nanorod structure before extensive membrane etching. The technique of growing TiO_2 nanorods in alumina membranes and sintering at 500°C with the nanorods still imbedded in the membrane offers excellent potential for obtaining TiO_2 nanorod arrays with extensive surface coverage on ITO glass substrates. Fig. 4C shows a cross-section of the TiO_2 nanorods, attached to ITO glass. Sintering the nanorods before attachment and membrane removal formed solid, rigid nanorods because the channel walls of the membrane acted as support structures for the nanorods during densification, which was critical for nanorod formation without deformation or distortion. Based on these SEM images, it can be seen that the nanorods are uniform, dense, and aligned unidirectionally, normal to the substrate surface.

Upon application of an appropriate electric potential, the charged nanoclusters in the sol will be drawn towards the cathode, eventually forming nanorods. It is postulated that the nanoclusters will fill the pores of the membrane, starting at the bottom, which is directly connected to the working electrode. In this manner, all the pores will eventually be completely filled. Prolonged deposition times lead to a layer of oxide forming on the membrane surface after the pores are filled. Upon heating the nanorods to an elevated temperature, densification will occur along with shrinkage. This explains why the observed diameter of the nanorods is smaller than that of the membrane pores. Although we do not know how closely the nanoclusters packed during the electrophoretic deposition, a lateral shrinkage of approximately 10–30% was observed when the nanorods were fired. Since the times and temperatures used are sufficient to form fully dense films from these sols, it is reasonable to assume that the nanorods are also nearly fully dense after firing. This in turn implies that near ideal close packing of nanoclusters might be achieved by this process. The existence of broken nanorods in first figures could be explained as follows. The polycarbonate membrane templates burn off at approximately 400°C in air, but the oxide nanorods are not likely to be fully dense (or crystallized) at this temperature, and thus have

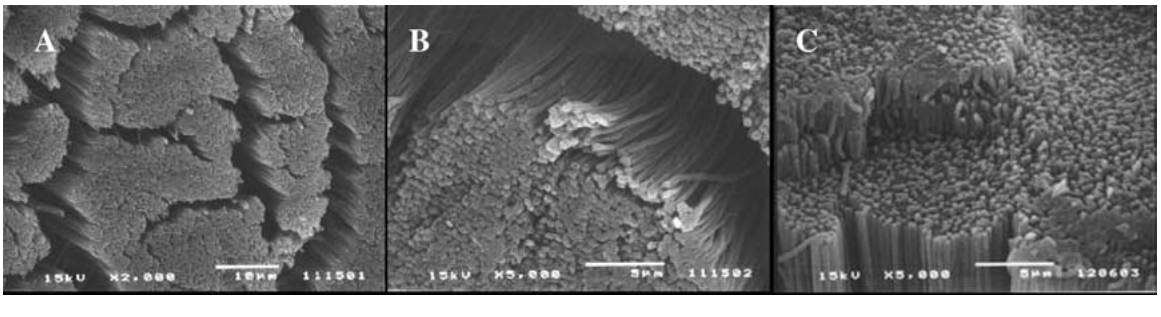

Figure 4 SEM images of (A) TiO_2 nanorod arrays, (B) individual TiO_2 nanorods, and (C) cross-section of TiO_2 nanorods attached to ITO conducting glass.

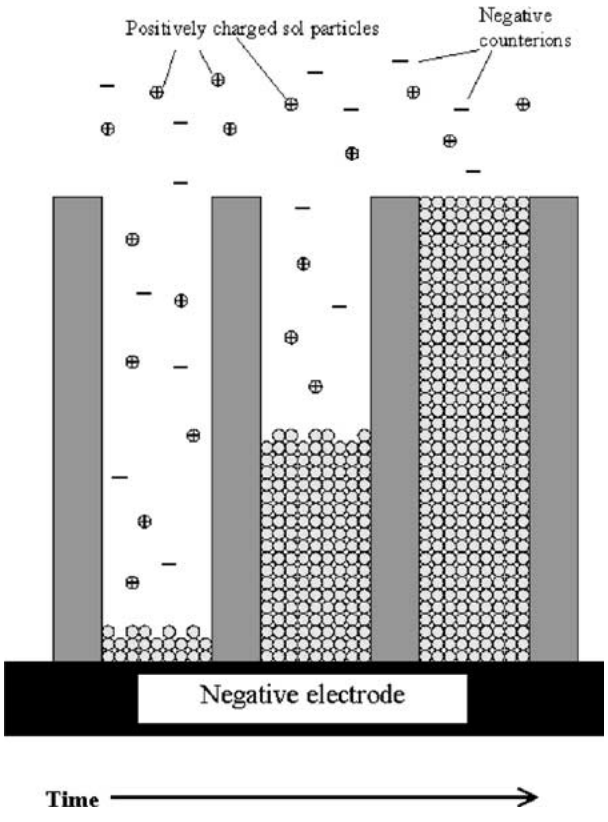

Figure 5 Schematic of the nanorod growth process, demonstrating the electrophoretic motion of charged oxide particles into the pores of the template membrane, filling the pores from the bottom up with time.

very limited mechanical strength. As the polycarbonate membrane and rods are heated, it is expected that some nanorods would break due to the differences in thermal expansion coefficients and distortion of the membranes. However, using alumina membranes could resolve this problem and would be advantageous for the formation of solid nanorods due to its high temperature resistance and non-deformation. In addition, as noted earlier, the use of longer drying times induces a greater degree of surface condensation between adjacent particles prior to firing of the samples. This in turn should make the samples stronger and more resistant to breakage during firing.

Fig. 5 is a schematic drawing of the electrophoretic deposition process. It demonstrates the steps we believe occur in the growth process. At the beginning of the nanorod growth, positively charged sol particles move due to electrophoresis towards the negative electrode. They deposit at the bottom of the pore, while the negatively charged counter ions move in the opposite direction. As time increases, the densely packed sol particles fill more of the pore, until the pore is completely filled. Dense cross-sections of TiO_2 nanorods observed by SEM and TEM, shown in Figs 1 and 2, suggest that the growth of oxide nanorods does indeed follow the mechanism proposed in Fig. 5. The results presented so far clearly demonstrate the ability of the sol electrophoresis technique to form nonconductive nanorods. Beyond this, however, there is no kinetic information about the process by which nanorod formation occurs. Monitoring the current that flows in the growth cell during nanorod formation can yield some insights into the growth process and kinetics of the electrophoresis.

Fig. 6A is a sample of the recorded current as a function of growth time for TiO_2 nanorods grown in a 100 nm polycarbonate template, with 5 V applied potential, and a spacing of 3 cm between the electrodes. From this data, one can see that the current rises quickly in the beginning of growth, and follows with a gradual increase after $\sim$1500 s. It is postulated that the initial sharp current rise corresponds to the filling of the template pores from the bottom through the template. As the template pores are being filled with TiO_2 nanoparticles or clusters, the distance that charged species, either ions or TiO_2 nanoclusters, must move through the small template pores decreases. This results in the drop of total resistance of the system, increasing the current. There is another possible mechanism leading to an increase in current due to the formation of a conductance path through the deposited TiO_2. Anatase is a wide band-gap semiconductor, and thus may conduct some of the current. It is possible that the resistivity of the deposited anatase is less than that of the anatase clusters moving in the sol, raising the current as the nanorods grow. After the pores are completely filled, the current rise with time is more gradual. This corresponds to the formation of a film of TiO_2 on top of the template. Other current measurement have been made (not shown), showing the effect of changing the pore size, sol concentration, and applied field. It was found that the overall current increases with increasing applied field, and that the time to reach a plateau in the current decreases. Similarly, decreasing sol concentration decreased the current, and slightly increased the time until the current plateau. Lastly, the effect of pore size was more difficult to explain. As expected, the total current decreases as the pore size decreases from 100 to 50 to 10 nm. However, the current for 200 nm pores is not larger than that for 100 nm pores, but lies about midway between that of 50 and 10 nm pores. One partial explanation for this may have to do with the pore densities of the various templates. The rated pore densities are 6×10^8 pores/cm^2 for all templates except the 200 nm, which have 4.5×10^8 pores/cm^2. This would lower the expected current, but not enough to account for the measured value. It is not know what caused this drastically reduced current value.

To see how the data fits with the proposed growth model, it is useful to calculate the current vs. time behavior for the growth model proposed, to see if it fits with the observed data. The current was calculated using a method similar to that used by Vandeperre and van der Biest [14], where the current path was broken into three sections, as shown in Fig. 7A. In each section, the resistance of the circuit is considered to consist of two parallel components. In Section 1, they are counter-ions diffusing through the pores of TiO_2 deposit and conduction of the TiO_2 deposit. In Sections 2 and 3, they are TiO_2 nanoparticles and counter-ions diffusing in the sol. Fig. 7B shows the equivalent circuit used to calculate the current. The resistances are:

$$R_{1,\mathrm{sol}} = \frac{\rho_{\mathrm{sol}} d_{\mathrm{l}}}{A_{\mathrm{p}} N_{\mathrm{p}}} \tag{1a}$$

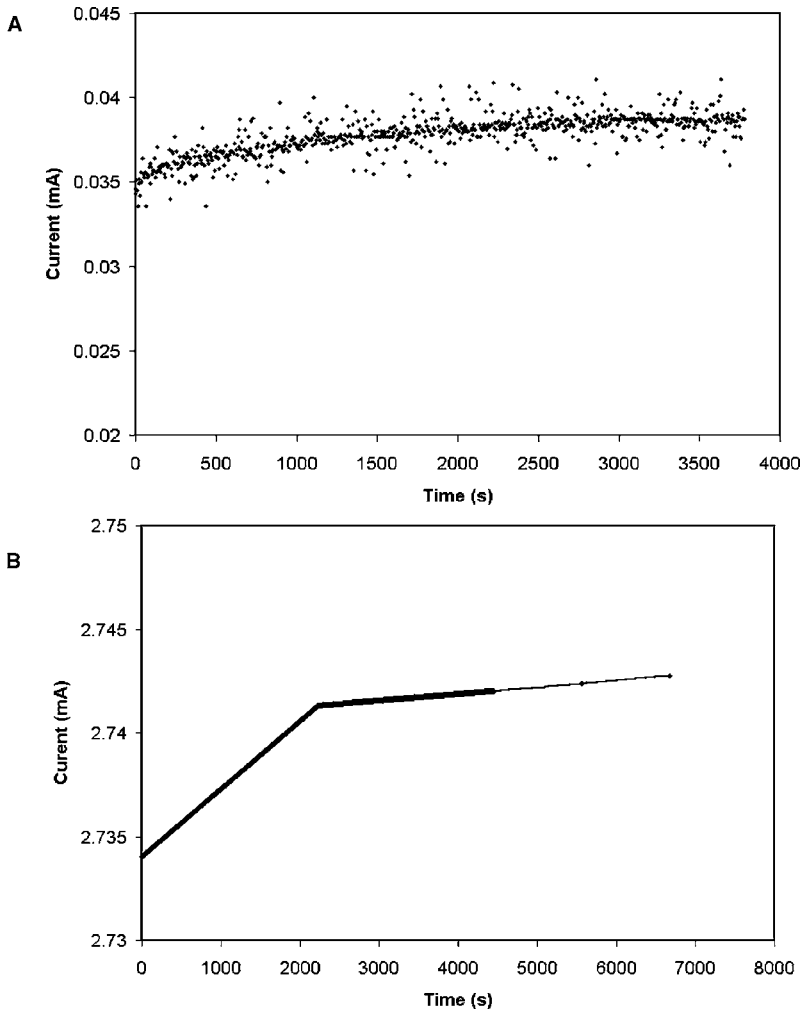

Figure 6 (A) is a sample of the recorded current as a function of time for TiO_2 nanorods grown in a 100 nm template at ~1.67 V/cm applied field. (B) is a sample calculation of the current for TiO_2 nanorods grown under the same conditions.

$$R_{1,\mathrm{p}} = \frac{\rho_{\mathrm{TiO_2}} d_\mathrm{l}}{A_\mathrm{p} N_\mathrm{p}} \tag{1b}$$

$$R_{2,\mathrm{sol}} = \frac{\rho_\mathrm{sol}(s - d_\mathrm{l})}{A_\mathrm{p} N_\mathrm{p}} \tag{1c}$$

$$R_{2,\mathrm{p}} = \frac{d - d_\mathrm{l}}{A_\mathrm{p} N_\mathrm{p} \mu Q c} \tag{1d}$$

$$R_{3,\mathrm{sol}} = \frac{\rho_\mathrm{sol}(d - s)}{A_\mathrm{c}} \tag{1e}$$

$$R_{3,\mathrm{p}} = \frac{d - d_\mathrm{l}}{A_\mathrm{c} \mu Q c} \tag{1f}$$

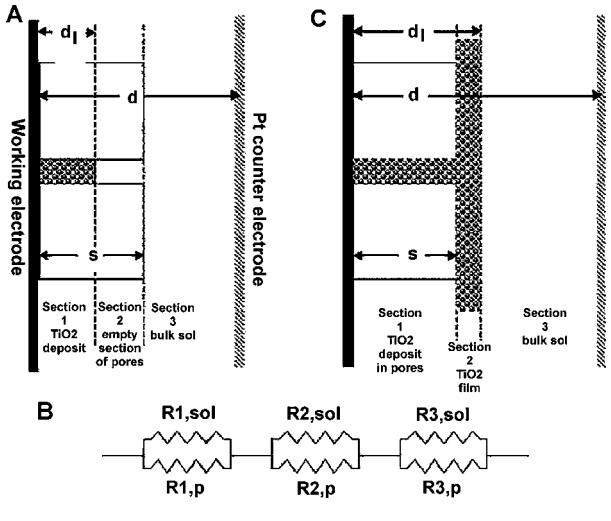

Figure 7 The models used in the current calculations: (A) the three sections of the growth process, for $d_\mathrm{l} < s$, (B) the equivalent circuit for part (A), and (C) the three sections of the growth process for $d_\mathrm{l} > s$.

where s is the thickness of the template, d_l is the thickness of the deposit, d is the distance between electrodes, A_p is the cross-sectional area per template pore, N_p is the total number of pores and A_c is the cross-sectional area of the growth cell. In the resistances, ρ_sol is the ionic resistivity of the sol, $\rho_{\mathrm{TiO_2}}$ is the resistivity of the TiO_2 deposit, μ is the mobility of the TiO_2 nanoparticles, Q is the effective charge per unit mass of the TiO_2 nanoparticles and c is the concentration of the sol. Because of the small volume of TiO_2 depleted from the sol (approximately ~1%) by nanorod growth, the concentration of the sol is assumed to remain constant. The values used for the other constants are: $\rho_\mathrm{sol} = 2.042\ \Omega\mathrm{m}$, $\rho_{\mathrm{TiO_2}} = 0.56\ \Omega\mathrm{m}$, $\mu = 1.01 \times 10^{-9}\ \mathrm{m^2/Vs}$ and $Q = 0.96\ \mathrm{C/kg}$. In this circuit, the resistances due to the electrodes and the interface reactions are neglected, as they are likely to be constant with time.

This circuit only applies for times up to the moment when the template pores are completely filled; after that, the system consists of three different sections as shown in Fig. 7C. For this circuit, the resistances in Sections 1 and 3 are similar to those above, modified for the fact that $d_l > s$. However, in Section 2 the resistances are similar to those in Section 1, with $A_p N_p$ replaced by A_c. Equation 1 gives the current as a function of the grown thickness, d_l, through Ohm's law. In order to compare the calculated currents to the observed values, it is necessary to have the current as a function of time. If the concentration is constant with time, the rate of mass deposition due to electrophoresis is [15]:

$$\frac{dM_{deposit}}{dt} = \rho_{deposit}\frac{dV_{deposit}}{dt} = \mu E A_{deposit} c \qquad (2)$$

with E being a function of time. For all times where $d_l < s$, the volume of the deposit can be calculated from the area of the template pores and the thickness of the deposit. An approximate solution of this equation gives:

$$t = \frac{\rho_{deposit}\lfloor d^2 - (d - d_l)^2 \rfloor}{2\mu V c} \qquad (3)$$

where V is the voltage drop across Sections 1 and 2, and can be calculated from the applied voltage (V_a) and current as:

$$V = V_a - I\left(\frac{1}{R_{1,sol}} - \frac{1}{R_{1,p}}\right)^{-1} \qquad (4)$$

A similar expression can be derived for $d_l > s$. Using Equations 1–4, one can calculate I and t as functions of d_l, and combine these to plot I as a function of t. A sample of such a calculation is shown in Fig. 6B, for TiO_2 grown in 100 nm templates at 5 V and 3 cm separating the electrodes. While the currents calculated by this method are much larger than those measured, they show the identical qualitative trend. That is, the current increases sharply up to the time when the template pores are completely filled, and then increases more gradually as a film of TiO_2 forms over the entire template. The calculated currents also show a qualitative agreement with measured values under different experimental conditions, such as changes in sol concentration or applied voltage. It was observed experimentally that samples grown for longer times have a thick film attached to the nanorods, while those grown for shorter times have little or no film. Both experimental results and calculation strongly supports the proposed model, for the growth of non-conductive oxide nanorods by electrophoresis that nanorod growth proceeds via motion of the nanoparticles to the bottom of the template pores, filling them up as time proceeds. Similar calculations have been performed for the various sol concentrations, applied fields and template sizes, showing the same type of agreement in all cases, except that (as mentioned above), the relative value of the current in 200 nm templates is calculated much higher than the measured value.

4. Conclusions

In summary, we have demonstrated the applicability of sol electrophoretic deposition to the creation of TiO_2 nanorods of various sizes, in different templates. TiO_2 nanorods with diameters in the range of approximately 45–200 nm and lengths of about 10–60 μm were grown in polycarbonate and alumina templates using sol-gel electrophoresis. By control of the sol preparation and sintering conditions, we have formed single-phase oxide nanorods of the desired composition and crystalline phase. Additionally, we have demonstrated the possibility of attaching TiO_2 nanorod arrays perpendicularly on a substrate such as ITO glass. Information about the steps occurring in the growth process was obtained by comparing calculated and measured currents in the electrophoretic cell. The calculated values were derived from a fairly simple model, and show good qualitative agreement with most of the experimental results. This supports the idea that growth occurs through the motion of charged nanoparticles to the bottom of the template pores, filling them up as time proceeds.

Acknowledgements

SJL and TPC acknowledge financial support from the Joint Institute for Nanoscience funded by the Pacific Northwest National Laboratory (operated by Battelle for the U.S. Department of Energy) and the University of Washington. SJL also acknowledges the Ford Motor Company fellowship.

References

1. J. CUI, A. WANG, N. L. EDELMAN, J. NI, P. LEE, N. R. ARMSTRONG and T. J. MARKS, *Adv. Mater.* **13** (2001) 1476.
2. M. A. PEÑA and J. L. G. FIERRO, *Chem. Rev.* **101** (2001) 1981.
3. E. STATHATOS, P. LIANOS, U. LAVRENCIC-STANGAR and B. OREL, *Adv. Mater.* **14** (2002) 354.
4. Y. LI, G. S. CHENG and L. D. ZHANG, *J. Mater. Res.* **15** (2000) 2305.
5. Z. W. PAN, Z. R. DAI, C. MA and Z. L. WANG, *J. Amer. Chem. Soc.* **124** (2002) 1817.
6. B. B. LAKSHMI, C. J. PATRISSI and C. R. MARTIN, *Chem. Mater.* **9** (1997) 2544.
7. B. CHENG and E. T. SAMULSKI, *J. Mater. Chem.* **11** (2001) 2901.
8. C. J. BRINKER and G. W. SCHERER, "Sol-Gel Science: The Physics and Chemistry of Sol-Gel Processing" (Academic Press, Boston, 1990).
9. W. D. CALLISTER, "Materials Science and Engineering: An Introduction" (John Wiley & Sons, New York, 1997).
10. S. J. LIMMER, S. SERAJI, M. J. FORBESS, Y. WU, T. P. CHOU, C. NGUYEN and G. Z. CAO, *Adv. Mater.* **13** (2001) 1269.
11. S. J. LIMMER, S. SERAJI, Y. WU, T. P. CHOU, C. NGUYEN and G. Z. CAO, *Adv. Funct. Mater.* **12** (2002) 59.
12. "Special Issue on Nanostructured Materials," *Chem. Mater.* **8** (1996).
13. "A Special Issue on Materials Science Aspects of Photonic Crystals," *MRS Bull.* **26** (2001).
14. L. J. VANDEPERRE and O. O. VAN DER BIEST, "Innovative Processing and Synthesis of Ceramics, Glasses, and Composites 1997" (American Ceramic Society, Westerville, Ohio, 1997) p. 261.
15. A. SIMONE and P. SPINELLI, *Mater. Eng.* **13** (2002) 33.

Received 20 January
and accepted 30 June 2003